

Sea ice melt drives vertical pCO₂ variability modulating air-sea gas exchange

Henry C. Henson^{1,2}, Dorte H. Søgaard^{2,3,7}, Bjarne Jensen⁶, Kunuk Lennert⁴, Tim Papakyriakou⁵, Mikael K. Sejr^{1,2}, Jakob Sievers⁶, Søren Rysgaard^{2,7}, and Lise Lotte Sørensen^{2,6}

¹Department of Ecoscience, Aarhus University, Aarhus, 8000, Denmark

²Arctic Research Center, Aarhus University, Aarhus, 8000, Denmark

³Greenland Climate Research Cluster, Greenland Institute of Natural Resources, Nuuk, 3900, Greenland

⁴UiT, The Arctic University of Norway, Tromsø, 9037, Norway

⁵Centre for Earth Observation Science, University of Manitoba, Winnipeg, MB, R3T 2N2, Canada

⁶Department of Environmental science, Aarhus University, Roskilde, 4000, Denmark

⁷Department of Biology, Center for Ice-free Arctic Research, Aarhus University, Aarhus, 8000, Denmark

Corresponding author: Henry C. Henson (hch@ecos.au.dk)

Key Points:

- Spring melting of sea ice and snow introduces distinct heterogeneity in surface water conditions within coastal Arctic oceans.
- Standard bulk parameterizations for air-sea CO₂ flux calculations, based on subsurface pCO₂ measurements, may misrepresent flux magnitude during melt periods.
- Vertical near-surface CO₂ and temperature gradients must be considered to improve flux estimates in stratified Arctic fjords.

30 **Abstract**

31 Strong spatial and temporal gradients in salinity, temperature, and carbonate chemistry in Arctic
32 coastal surface waters complicate the estimation of air-sea carbon dioxide (CO₂) exchange,
33 particularly during sea ice breakup. The present study evaluates the applicability of the widely
34 used bulk flux model under such conditions. This approach assumes homogeneous surface
35 conditions and no vertical pCO₂ gradients in the bulk seawater. However, our observations in a
36 stratified Arctic fjord reveal pronounced vertical variability in pCO₂ within the upper water
37 column, including non-linear gradients near the air-sea interface. This results in, widely varying
38 flux estimates depending upon the depth of the pCO₂ measurement used to establish air-sea
39 disequilibrium. These findings highlight the importance of resolving near-surface variability
40 during the transition from ice-covered to open water conditions. We recommend incorporating
41 both micrometeorological techniques and high-resolution vertical profiling in Arctic fjords to
42 improve flux estimates of CO₂ in this rapidly changing region.

43

44 **Plain Language Summary**

45 Sea ice melt adds less-saline water to the surface ocean. This creates vertical gradients in
46 salinity, temperature, and partial pressures of carbon dioxide (pCO₂). The concentration
47 difference of pCO₂ across the air-ocean boundary is used to estimate gas transfer. Thus, the
48 depth that we measure will impact our estimates. This means ocean layering during ice melt may
49 slow or briefly reverse the direction of CO₂ transfer.

50

51 **1 Introduction**

52 High latitude coastal oceans are strong sinks for atmospheric carbon dioxide (CO₂), absorbing
53 more CO₂ per unit area than lower latitude regions (Dai et al., 2022; Roobaert et al., 2019). This
54 strong uptake results from both the high solubility of gases in cold water and the intense
55 biological activity typical of these regions. However, climate change is rapidly transforming this
56 carbon sink. The Arctic is warming more than twice as fast as the global average, and sea ice
57 extent has been shrinking by over 13% per decade (Perovich et al., 2020). The loss of sea ice
58 increases CO₂ uptake by exposing larger areas of open water for longer periods, which can
59 further stimulate biological productivity (Arrigo and van Dijken, 2015; Bates and Mathis, 2009;
60 Perovich et al., 2020). However, at the same time, melting sea ice freshens the surface layer and
61 strengthens stratification, limiting vertical mixing with deeper water. Freshwater from melting
62 sea ice and terrestrial run-off creates pronounced gradients in physical properties such as salinity
63 and temperature, as well as chemical properties like dissolved inorganic carbon (DIC) and total
64 alkalinity (TA) (e.g. Henson et al., 2025). As a result, the partial pressure of CO₂ (pCO₂) can
65 vary markedly with depth under melt conditions (Miller et al., 2019).

66

67 This vertical variability in pCO₂ poses a challenge for air-sea CO₂ flux estimation. The transfer
68 of gases between the atmosphere and ocean depends on the difference in concentration between
69 the two as well as the efficiency of the transfer process. Therefore, the bulk flux of CO₂ across

70 the air-sea interface is commonly described as the product of the gas transfer velocity, k (m s^{-1}),
71 CO_2 solubility s ($\text{mol kg}^{-1} \text{atm}^{-1}$), and the partial pressure gradient (μatm) across the air-sea
72 interface (Wanninkhof et al., 2009):

73

$$74 \quad F = ks(p\text{CO}_{2_{sea}} - p\text{CO}_{2_{air}}) \quad (1)$$

75

76 While widely applied, this formulation simplifies a complex process influenced by surfactants on
77 the water surface, bubble-mediated gas exchange, and turbulence (Wanninkhof et al., 2009).
78 Furthermore, surface water heterogeneity, driven by sea ice melt and freshwater runoff from
79 land, complicate the physical and chemical processes governing air-sea CO_2 exchange. As a
80 result, simplified parameterizations commonly used in global carbon flux estimates may be
81 inadequate in these settings.

82

83 In most studies, $p\text{CO}_2$ is measured several meters below the surface, assuming vertical
84 homogeneity under well-mixed condition (Jørgensen et al., 2020). However, in stratified waters,
85 where temperature, salinity, and pH can vary with depth, this assumption may lead to substantial
86 errors in flux estimates (Ahmed et al., 2020; Dong et al., 2021; Miller et al., 2019; Watts et al.,
87 2022). Although Arctic surface waters are often undersaturated with respect to atmospheric CO_2
88 levels and act as CO_2 sinks (e.g., Burgers et al., 2017; Dai et al., 2022; Henson et al., 2024;
89 Laruelle et al., 2014; Roobaert et al., 2019), such assessments typically rely on sparse data
90 collected from 0.5-5 m depth during limited periods. Dong et al. (2021) illustrate that high
91 latitude fluxes of CO_2 calculated using the bulk method (based on measurements sampled at 6 m
92 depth) differ significantly from those measured using direct eddy covariance in sea ice melt
93 regions.

94

95 Gas transfer velocity (k) is often parameterized as a function of wind speed. However, the true
96 driver is mixing in the surface waters, which governs k . Fick's first law of diffusion, which
97 underlies Equation (1), assumes a linear concentration gradient within the diffusive sublayer
98 (Fig. 1) and steady-state conditions (Garbe et al., 2014). Jørgensen et al. (2020) argued that, due
99 to seawater's high buffer capacity, chemical gradients do not significantly affect CO_2
100 equilibration, supporting the use of measurements at 3-4 m depth. However, this conclusion
101 relies on the assumption of horizontal and vertical homogeneity and neglects the effects of
102 shallow surface stratification, particularly when alkalinity dilution is involved.

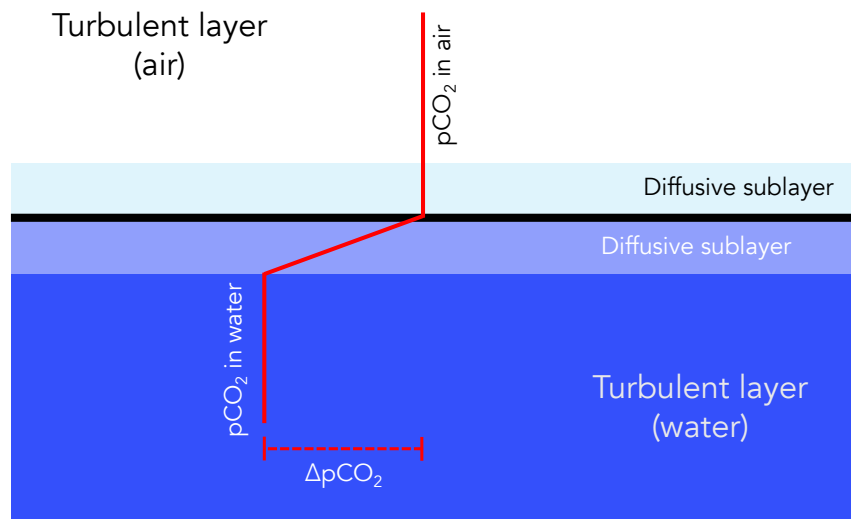
103

104 In Arctic spring, the upper ocean is often strongly stratified due to freshwater input from glacier
105 melt, snowmelt, river runoff, and sea ice meltwater (Ahmed et al., 2020; Granskog et al., 2011;
106 Meire et al., 2017; Miller et al., 2019). These inputs can extend vertical CO_2 gradients beyond
107 the diffusive sublayer, complicating flux estimates during ice breakup and early open-water
108 periods. Several studies have demonstrated strong vertical heterogeneity in $p\text{CO}_2$ in Arctic

109 coastal waters, with implications for air-sea flux calculations (Ahmed et al., 2020; Dong et al.,
110 2021; Miller et al., 2019).

111 Surface freshening from ice melt and runoff strongly influences carbonate chemistry in Arctic
112 coastal waters, which can either suppress or enhance oceanic CO₂ uptake. For example, Burgers
113 et al. (2017) reported large horizontal variability in surface pCO₂ (144–364 μatm) linked to
114 riverine input in the Eastern Canadian Arctic. Similarly, Sejr et al. (2011) observed strong
115 surface pCO₂ gradients associated with salinity and temperature in Young Sound, and later
116 documented a long-term decline in surface salinity (Sejr et al., 2017). Freshwater-induced
117 stratification has also been shown to create vertical gradients in pCO₂ and pH with important
118 implications for flux calculations (Miller et al., 2019). Finally, Bates et al. (2014) demonstrated
119 that sea ice meltwater and melt ponds exhibit extreme variability in pCO₂ (<10 to >1500 μatm)
120 and pH (6.1 to >10.8), highlighting the complex chemical landscape of ice-influenced waters.
121 Together, these studies underscore the high spatial and temporal variability of carbonate
122 chemistry in freshened waters across the Arctic.

123 To project future CO₂ uptake or outgassing in the Arctic, we must better understand the physical
124 and chemical drivers of near-surface carbonate variability. In this study, we investigate the
125 vertical and temporal variations in pCO₂ in a stratified Arctic fjord during sea ice breakup. By
126 examining water-column pCO₂ profiles across the transition from ice-covered to open water, we
127 evaluate usage of the bulk flux model under Arctic seasonal transitions.
128



129
130 **Figure 1.** Schematic illustrating the interface between the air and the water in conjunction with
131 pCO₂ concentration gradients. In equation 1, the concentration gradient is assumed to occur in the
132 diffusive layer between the air and water, and the concentrations are assumed to be vertically
133 constant in the turbulent layers. (Adapted from Liss and Slater, 1974; Wanninkhof et al., 2009)
134

135 2. Study Site and Measurement Methods

136

137 **2.1 Study Site**

138 This study was conducted in Young Sound, a high Arctic fjord system located near the Daneborg
139 Research Station in Northeast Greenland (Fig. 2). The fjord system comprises the Tyrolerfjord
140 (inner fjord) and Young Sound (outer fjord), extending approximately 90 km from Tyroler River
141 to the Greenland Sea. A sill at about 45 m depth separates Young Sound from the open ocean.
142 Young Sound is 2 to 7 km wide, with an average depth of 100 m (maximum 350 m), and a total
143 surface area of ~390 km². Tidal amplitudes range from 0.8 to 1.5 m, with mean current velocities
144 of approximately 2 cm s⁻¹ (Rysgaard et al., 2003). Freshwater inputs are primarily derived from
145 Greenland Ice Sheet runoff, local glaciers, precipitation, and snowmelt from adjacent ice-free
146 terrain. The drainage basin of the Tyrolerfjord/Young Sound system spans 2846 km², of which
147 33% is glaciated.

148

149 Sampling was conducted from 12 to 31 July 2017. Sampling occurred during and immediately
150 after a period of sea ice breakup. On 15 July, ice coverage was approximately 30%, decreasing to
151 less than 10% by 16 July. Water sampling was conducted both from an inflatable boat and via
152 sea ice leads, all in close proximity to the Greenland Ecosystem Monitoring (GEM) program's
153 standard station (Fig. 2).

154

155 **2.2 pCO₂ Measurements Using the HydroC Sensor**

156 Surface water pCO₂ was measured with a CONTROS® HydroC CO₂ sensor, which utilizes a
157 membrane equilibrator coupled with a non-dispersive infrared detector. The instrument is
158 equipped with a built-in water pump that provides flow rate of 35 ml s⁻¹ across the membrane. At
159 each sampling depth, the sensor was allowed to equilibrate for 10 to 20 minutes, and values were
160 recorded once stable for at least two minutes. The sensor operates over a range of 200-1000 µatm
161 and temperatures of -2 to 35°C. Annual calibration has been conducted using a certified 400 ±
162 2% ppm CO₂ gas that was traceable to WMO standards. The sensor showed remarkable stability
163 (397-401 ppm), supporting a measurement uncertainty of ± 2 µatm.

164

165 **2.3 pCO₂ Estimation from TA and DIC**

166 In addition to direct measurements, pCO₂ was calculated from total alkalinity (TA) and dissolved
167 inorganic carbon (DIC) using the Seacarb package (Gattuso et al., 2024) in R. Due to the low
168 salinity and cold temperatures characteristic of Arctic coastal waters, no universally accepted set
169 of equilibrium constants (K1 and K2) exists. For consistency with previous studies in the region
170 (Henson et al., 2023), we used the refitted constants from (Lueker et al., 2000). The selection of
171 equilibrium constants introduces assumptions regarding seawater composition. (Raimondi et al.,
172 2019) showed that different constants can lead to discrepancies between measured and calculated
173 pCO₂ values, ranging from -3.1 to -35.8 µatm, with Lueker et al. (2000) demonstrating the best
174 internal consistency under polar conditions. Still, (Sulpis et al., 2020) found that the calculation

175 of pCO₂ from DIC and TA can lead to uncertainty up to 15% under cold conditions, which is far
176 greater than when pCO₂ is measured directly.

177

178 **2.4 Sea Ice TA and DIC Sampling**

179 TA and DIC in sea ice were assessed using three ice cores. Each core was sectioned into 5-10 cm
180 segments and sealed in gas-tight NEN/PE bags with sampling valves (Hansen et al., 2000).
181 Samples were transported in thermally insulated boxes to a nearby field laboratory. Cold (1°C)
182 deionized water of known mass and carbonate composition (10 - 30 ml) was added to each bag,
183 which was then resealed after removing air and weighted.

184

185 The samples were melted in the dark over ~48 hours. Meltwater was transferred to 12 mL
186 Exetainer vials (Labco, UK) pre-dosed with 20 µl of saturated HgCl₂ solution (5% w/v) to
187 prevent microbial alteration. DIC was measured by on Apollo SciTech®'s AS-C3 analyzer while
188 TA was determined via potentiometric titration on an Apollo SciTech AS-ALK2 total alkalinity
189 titrator (Haraldsson et al., 1997).

190

191 **2.5 Physical Parameters**

192 Vertical profiles of conductivity, temperature, and depth (CTD) were obtained using a Seabird®
193 SBE19plus CTD. On 16 July 2017, additional surface conductivity measurements were taken
194 using a Thermo Orion-Star® instrument with an Orion 013610MD conductivity cell. Surface
195 water temperatures were independently measured with a Testo® thermometer.

196

197 **2.6 Historical Data**

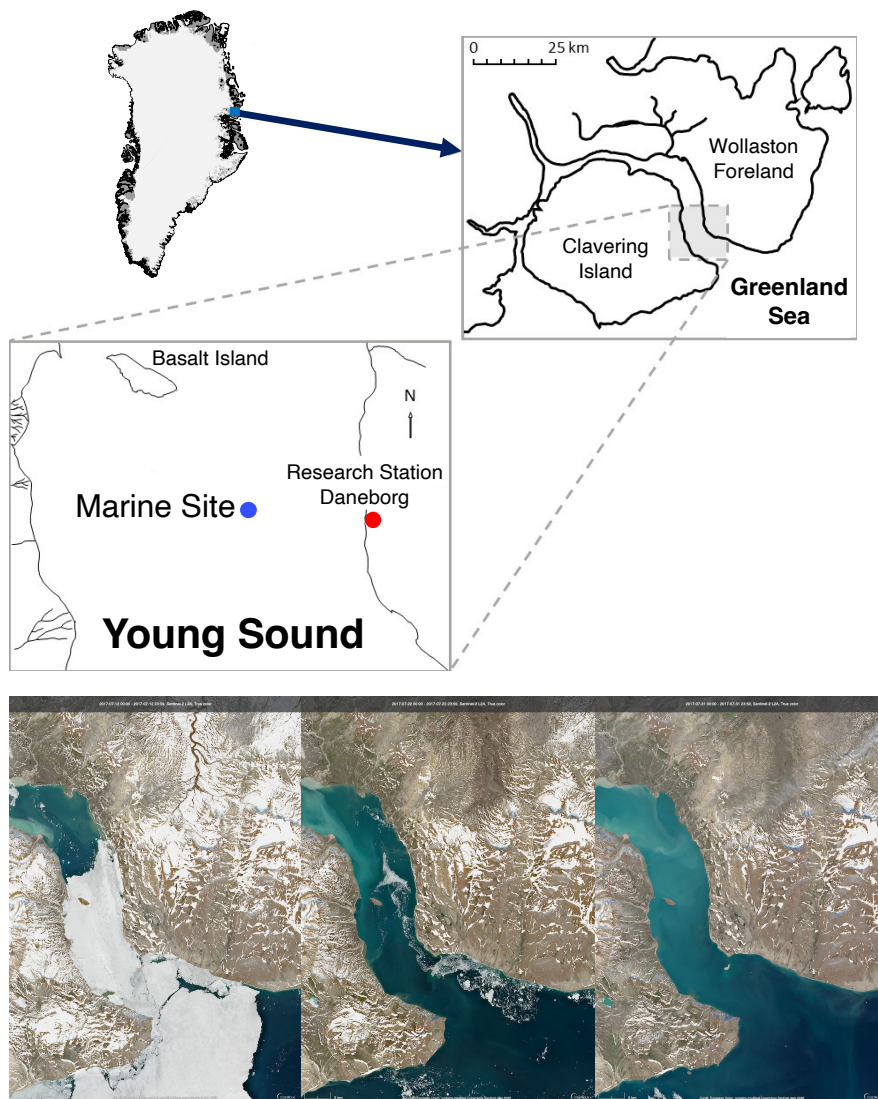
198 For contextual comparison, pCO₂ time series data from the Greenland Ecosystem Monitoring
199 program are also included in the analysis. pCO₂ data from 2007-2023 was measured using the
200 same HydroC CO₂ sensor in August each year.

201

202 **2.7 Eddy Covariance**

203 Sensible and latent heat fluxes were estimated using micrometeorological instrumentation
204 mounted on a 3-meter mast positioned approximately 0.5 meters from the waterline. Three-
205 dimensional wind vectors were recorded using a METEK® uSonic-Scientific sonic anemometer.
206 To enhance reliability, we applied complementary analysis techniques for flux estimation: (1) the
207 standard eddy covariance (EC) method using EddyPro software (Version 7.0.6, LI-COR Inc.,
208 2019); (2) the ogive optimization method (OGM) (Sievers et al., 2015a). Among these, the OGM
209 was deemed most robust due to its ability identify and filter out low-frequency noise, sensor
210 dampening, and large-scale turbulent motions that can bias flux measurements. These issues
211 often introduce large relative bias associated with flux measurement over Arctic marine surfaces
212 (Sievers et al., 2015b). OGM's superior ability to isolate relevant turbulent scales and reduce
213 contamination from mesoscale variability is based on the accumulation and modelling of each
214 cospectra over each 20 min averaging period (Fig. S1 and S2). Uncertainty in sensible and latent

215 heat fluxes was estimated directly from the OGM procedure. The reported values correspond to
216 the standard error associated with the fitted ogive tail and reflect random uncertainty in flux
217 integration.
218



219
220
221 **Figure 2.** Map of Greenland and the sampling area at the coast of Young Sound in Northeast
222 Greenland. The red circle indicates the location of the micrometeorological measurement tower
223 at research station Daneborg while the marine sampling site (Standard Station in the Greenland
224 Ecosystem Monitoring program) is indicated as a blue circle (74.310, -20.300). Three
225 Copernicus Sentinel true-color images of the fjord on July 12, 22, and 31 illustrate the transition
226 between sea ice cover and open water.

227
228 **3 Data and results**
229

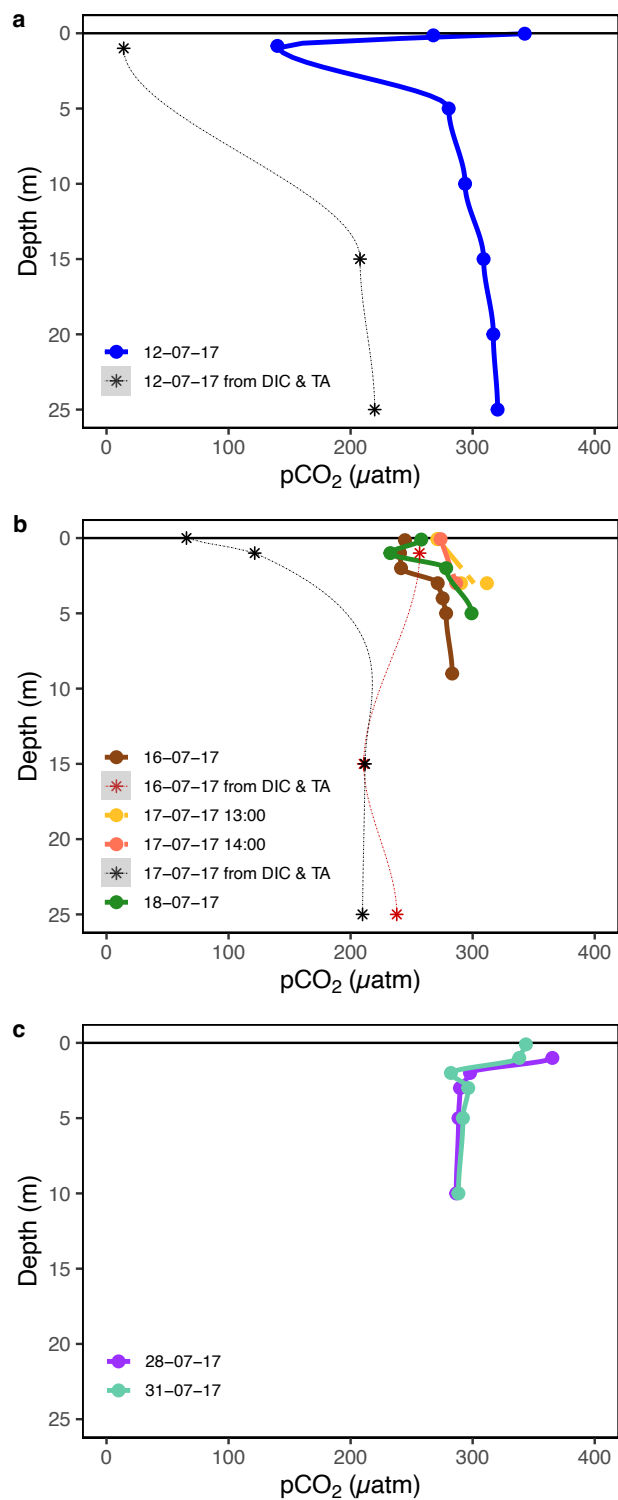
230
231
232
233
234
235
236
237
238
239
240
241
242
243
244
245
246
247
248
249
250
251
252
253
254
255
256
257
258
259
260
261
262
263
264
265
266
267
268
269

Vertical profiles of surface water pCO₂ were measured using the CONTROS® HydroC CO₂ sensor across three distinct periods in July 2017 (Fig. 3a-c). Each observational period corresponded to different sea ice conditions: before, during and after sea ice breakup (Fig. 2). These high-resolution profiles revealed substantial vertical variability within the upper 2 to 3 meters of the water column. Under ice-covered conditions, pCO₂ measurements were taken through an open melt pond. At this time, elevated CO₂ concentrations were observed at the very surface (0.1 m), followed by a sharp decrease to approximately 1 meter depth, coinciding with the ice-water interface. Below this depth, pCO₂ increased again, though remained well below atmospheric concentrations (Fig. 3a).

During the period of sea ice breakup, when ice coverage ranged from approximately 30% to 10%, the vertical distribution of pCO₂ exhibited a similar structure. Concentrations were highest near the surface, declined to a local minimum at 1 to 2 meters, and then stabilized below 3 meters (Fig. 3b). Following, the complete breakup of sea ice, pCO₂ showed a more gradual decrease from the surface down to about 3 meters, beneath which concentrations remained relatively constant (Fig. 3c). Across all three observational periods, a shallow surface layer approximately 5 m thick was identified, within which most of the pCO₂ variability occurred. Below this depth, pCO₂ remained relatively constant.

These vertical structures are consistent with strong physical stratification, likely driven by freshwater input from glacial melt and surface heating. Temperature and salinity profiles collected concurrently support the presence of sharp vertical gradients in the upper water column, with salinity ranging from 1.4 to 29.6 PSU and temperature from -0.4°C to 6.2°C. These physical profiles, shown in Fig. 4, confirm that vertical mixing was strongly suppressed during the observational period. The small tides present in Young Sound, combined with the continued input of freshwater from first sea ice and then glacial melt, lead to a fjord system with distinct surface stratification throughout the months of July and August.

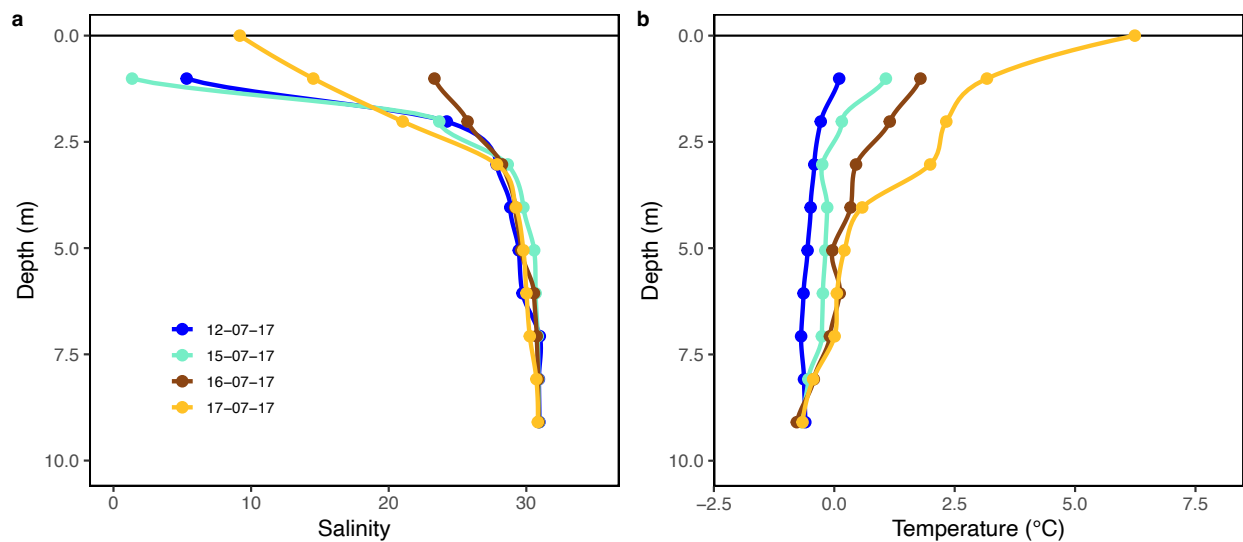
Measurements from a different fjord in East Greenland on June 4, 2025, revealed strikingly similar vertical pCO₂ heterogeneity (Fig. 5). Elevated pCO₂ at 0.1 m decreased to a minimum around 1-1.5 m before increasing again and stabilizing near 3 m depth. Extreme stratification in the upper few meters caused pCO₂ levels in each profile to vary by more than 100 µatm between the surface and 1 m. This repeated observation of comparable vertical pCO₂ heterogeneity 8 years later and in a different fjord system suggest this is not an isolated phenomenon. Indeed, Arctic surface stratification during sea ice breakup induces chemical changes that may influence the way we estimate air-sea exchange of CO₂.



271
272

273 **Figure 3.** Measured Young Sound $p\text{CO}_2$ profiles (a) prior to sea ice breakup (measured through
274 open melt pond), (b) during sea ice breakup and (c) after sea ice break up measured through CO_2
275 equilibration and calculation from carbonate chemistry parameters (DIC & TA).

276

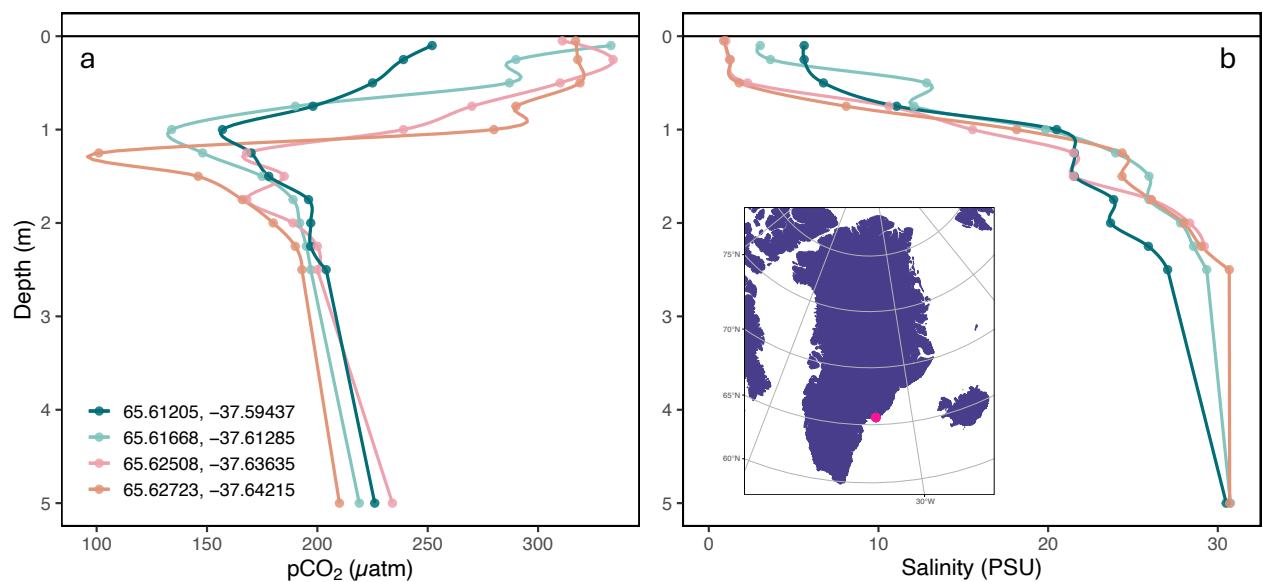


277

278

279 **Figure 4.** Measured Young Sound profiles of under-ice water and open water salinity and
280 temperature.

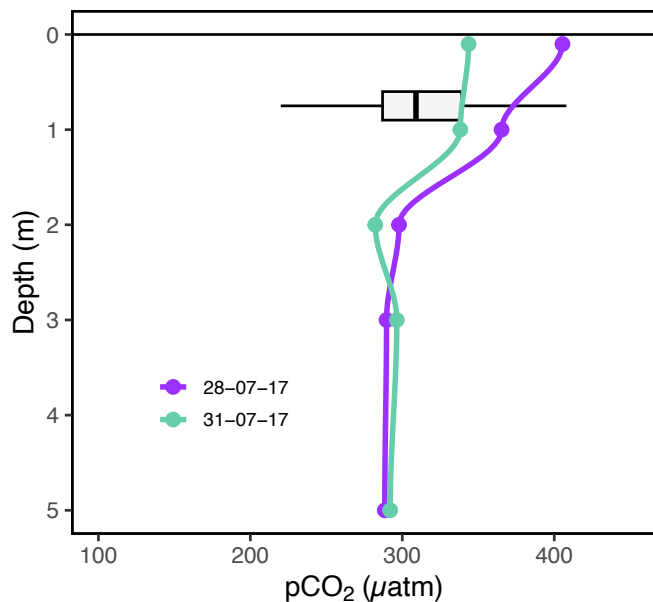
281



282

283

284 **Figure 5.** Measured pCO₂ (a) and salinity (b) profiles at 4 locations in Tasiilaq Bay. Profiles
285 were measured on June 4, 2025 during the period of sea ice breakup following the method in Sejr
286 et al. (2011).



287
288

289 **Figure 6.** Measured Young Sound pCO₂ profile after ice break up in 2017 compared with historical
290 variation in pCO₂ at 1 m depth in the same location.

291
292

293 4. Discussion

294 Air-sea CO₂ fluxes in Arctic coastal areas are generally estimated using bulk parameterization
295 models (Henson et al., 2024; Meire et al., 2015; Roobaert et al., 2019; Sejr et al., 2011). These
296 models rely on several key assumptions, including unstratified surface conditions, a linear pCO₂
297 gradient within the diffusive boundary layer, and a vertically uniform pCO₂ profile within the
298 mixed layer. Our observations challenge the applicability of these assumptions in Arctic coastal
299 waters in several important ways. We observe distinct vertical heterogeneity in both physical and
300 chemical parameters, which leads to distinct differences in flux estimates based on the depth of
301 the measurements used.

302

303 4.1. Stratified conditions in the marine CO₂ system

304 Vertical pCO₂ profiles collected during July 2017 revealed pronounced non-linear behavior in
305 the upper 3 to 5 meters of the water column (Fig. 3). This directly contradicts the assumption that
306 the ΔpCO₂ accurately represents the difference between the atmosphere and the “well-mixed
307 bulk fluid” below the diffusive layer (Wanninkhof et al., 2009). Under ice-covered conditions,
308 the lowest pCO₂ values (~150 ppm) were consistently observed just beneath the sea ice, with
309 concentrations increasing with depth and stabilizing around 5 m (Fig. 3a). During the ice breakup
310 stage, a similar pattern emerged, although the minimum pCO₂ was higher (~250 ppm).

311

312 More recent measurements from Tasiilaq Bay in June 2025 demonstrate very similar vertical
313 pCO₂ profiles. Indeed, 4 high-resolution profiles with measurements every 0.25 m reveal the

314 same C-shaped pCO₂ variation. Like in Young Sound, the most elevated pCO₂ levels were
315 observed near the surface, and pCO₂ minimums occurred near 1-2 meters depth before increasing
316 and becoming stable. This repeated observation in a different fjord system, but during the period
317 of sea ice breakup indicates this vertical variability may be representative during stratified Arctic
318 conditions.

319
320 Several interacting processes influence surface water chemistry during ice breakup. Low surface
321 water pCO₂ values reflect the influence of low-salinity meltwater from snow and sea ice or
322 glacial meltwater found in freshened Arctic waters (Geilfus et al., 2015; Henson et al., 2025).
323 However, surface water chemistry during the ice breakup period is further complicated by
324 processes such as ikaite (CaCO₃·6H₂O) dissolution (Miller et al., 2011; Rysgaard et al., 2013;
325 Søgaard et al., 2013) and high under-ice primary production (Søgaard et al., 2021). Additionally,
326 snowmelt, characterized by low pH and ionic strength (de Caritat et al., 2005), may further alter
327 carbonate system dynamics in the upper water column.

328
329 Two mechanisms may explain the nonlinear C-shaped trend in pCO₂ observed in the top few
330 meters. First, as demonstrated by Henson et al. (2025) mixing between glacial meltwater and
331 seawater can result in nonlinear behavior in pCO₂, even when DIC and TA mix conservatively.
332 In such cases, initial freshwater dilution leads to dramatically reduced pCO₂, but at very low
333 salinities, the diminished buffering capacity can cause acidification to occur and pCO₂ to
334 increase again. In fact, Henson et al. (2025) present a U-shaped pCO₂ curve along a salinity
335 gradient that appears extraordinarily similar to the C-shaped pCO₂ curve we observe with depth.
336 Indeed, the salinity gradient created in their mixing experiments can be observed vertically in the
337 highly stratified surface waters during sea ice breakup (Fig. 3a, 5a). Although, Henson et al.
338 focused on the influence of glacial meltwater, our results suggest similar processes could occur
339 in systems influenced by sea ice and snowmelt.

340
341 Both glacial meltwater and sea ice have low DIC concentrations and act to dilute the inorganic
342 carbon of the surface ocean (Fig. S4). However, changes in alkalinity can also impact the
343 buffering capacity of the water mixture, leading to nonlinear effects. If the meltwater has a lower
344 TA:DIC ratio than seawater, due to the absence of ikaite, acidification and a shift in carbonate
345 equilibria at very low salinities could lead to higher pCO₂ values at the surface. During July
346 2017, Young Sound showed both diluted DIC and TA levels in upper few meters, suggesting pH
347 change during sea ice break up could occur more easily (Fig. S4). Indeed, calculated pH profiles
348 indicated variable surface conditions between periods of sea ice cover and sea ice breakup (Fig.
349 S5). In this very fresh surface layer, diminished pH may elevate pCO₂ relative to waters around 1
350 m depth, where freshwater-seawater mixing ratios are more moderate and seawater buffering
351 leads to very low CO₂ concentrations.

352

353 A second, but less likely, explanation involves atmospheric equilibration of sea ice melt ponds
354 before draining into open leads. The relatively elevated $p\text{CO}_2$ observed at ~ 0.1 m depth could
355 reflect such partial equilibration. While chamber-based studies (e.g. Geilfus et al., 2012, 2015;
356 Nomura et al., 2010; Semiletov et al., 2004) have demonstrated both uptake and efflux of CO_2 in
357 melt ponds, equilibrium times between melt-pond water and atmosphere depend upon pond
358 depth, wind speed, and carbonate chemistry. For example, a 0.1 m deep pond under low wind
359 conditions ($\sim 2 \text{ m s}^{-1}$) may reach atmospheric equilibrium in 1-4 days. However, in our case,
360 $p\text{CO}_2$ values calculated from TA and DIC in melt ponds did not indicate equilibrium with the
361 atmosphere, making this explanation less likely than the freshwater mixing mechanism.
362 Nevertheless, atmospheric equilibration may play a role after the sea ice barrier is removed.
363 Elevated $p\text{CO}_2$ levels at the surface (0.1 m) post sea ice breakup may result from the
364 combination of the chemical changes described above, heating from solar radiation, and from
365 atmospheric CO_2 uptake (partial equilibration) in the limited volume of this freshwater lens.

366
367 As melt progresses and sea ice recedes, riverine input and vertical mixing become more
368 influential. Yet even after ice breakup, surface waters often remain fresh due to glacial meltwater
369 runoff, and the resulting low salinities help maintain stratification. In August 2017, vertical
370 structure remained pronounced even after sea ice breakup, with elevated $p\text{CO}_2$ at 0.1 m which
371 stabilized below ~ 3 m. In other words, near-surface conditions remained decoupled from deeper
372 waters. This persistent shallow layer, characterized by low salinity, higher temperature, and
373 elevated $p\text{CO}_2$, suppresses gas exchange with the colder, more undersaturated water below,
374 consistent with observations by Dong et al. (2021). In such environments, bulk flux models that
375 assume homogeneity and linear gradients are likely to yield biased or inaccurate estimates.

376 To place these 2017 measurements in historical context, we examined long-term surface water
377 $p\text{CO}_2$ data collected at 0.5-1 m depth by the Greenland Ecosystem Monitoring (GEM) program
378 between 2007 and 2023. These data, measured using consistent protocols, are presented in Fig. 6
379 alongside our open-water profiles. Over the 17-year record, August $p\text{CO}_2$ concentrations at ~ 1 m
380 depth had ranged from 220 to 408 μatm and had consistently remained below atmospheric levels.
381 This apparent stability has contributed to the perception of sustained CO_2 uptake throughout the
382 summer season. However, the high-resolution vertical profiles obtained during the 2017 field
383 campaign add nuance to this assumption. Elevated $p\text{CO}_2$ levels confined to the uppermost meter
384 of the water column may go undetected in standard monitoring approaches that rely on fixed-
385 depth sampling. These results suggest that the dynamic changes during sea ice melt can induce
386 episodes of slowed uptake, air-sea equilibrium, or CO_2 outgassing. Consequently, existing
387 sampling protocols may underestimate surface variability and bias flux estimates, especially in
388 stratified conditions where near-surface chemistry is decoupled from subsurface layers.

389
390 **4.2. Influence of surface stratification on fluxes**

391 To assess how bulk models function when estimating CO₂ fluxes in an Arctic fjord influenced by
392 sea ice and snow melt, we calculated fluxes using seawater pCO₂ measurements from multiple
393 depths and two gas transfer velocity parameterizations. Specifically, we computed fluxes
394 throughout July using pCO₂ measured at 0.1, 1, 2, and 4 m. To estimate the surface (interface)
395 pCO₂ at 0 m, we adjusted the 1 m pCO₂ measurements to a derived skin temperature (Table 1),
396 estimated from sensible heat fluxes (Fig. S6) following the parameterization of Smedman et al.
397 (2007). Accounting for this skin layer correction is critical, as Woolf et al. (2016) demonstrated
398 that neglecting the thermal skin and relying only on bulk sea surface temperature can introduce
399 significant errors in flux estimates.

400

401 The resulting calculations (Table 1) show that estimated CO₂ fluxes vary significantly depending
402 on the depth of the pCO₂ measurement. Notably, fluxes derived from 0.1 m differ markedly from
403 those based on deeper values. Since many studies rely on pCO₂ measured at a fixed depth (often
404 at 1 m or at a ship's seawater intake below 5 m), these results underscore the potential for
405 misrepresentation of flux magnitude and direction due to vertical heterogeneity in surface water
406 chemistry.

407

408

409 Measurements from both Young Sound and Tasiilaq demonstrate that during sea ice breakup,
410 pCO₂ levels are most elevated at the surface. This may be linked to acidification of the most
411 freshened 0.5 m and a shift in the marine carbonate system, or partial equilibration due to air-sea
412 gas transfer. If this acidified freshwater lens warms, for instance, due to solar radiation, pCO₂
413 may rise leading to oversaturation relative to atmospheric concentrations. Indeed, when pCO₂
414 measurements on July 31 were corrected for skin temperature, to estimate pCO₂ at the boundary
415 layer, they suggested a transition from undersaturation to oversaturation (Table 1). While we did
416 not directly observe this oversaturation in the vertical profiles, this likely reflects the inability to
417 sample at the sea surface. Nevertheless, the occurrence of stratification-related vertical pCO₂
418 heterogeneity, with levels most elevated at the surface, will slow air-sea gas transfer compared to
419 when conditions are well mixed. Meanwhile, warming or acidification of the thin surface layer
420 may periodically induce a reversal of flux direction, as seen in some micrometeorological studies
421 in Arctic coastal environments during sea ice breakup (e.g. Butterworth et al., 2025).

422

423

424 Overall, these findings echo those of Miller et al. (2019), who reported pronounced spatial
425 heterogeneity in Arctic coastal pCO₂ and large differences in estimated fluxes depending on the
426 sampling depth. The broader implications of this heterogeneity for seasonal or regional flux
427 estimates remain unclear. However, if fluxes are upscaled from sparse, single-point
428 measurements (e.g., once per month, as in Laruelle et al., 2014), substantial errors may result due
429 to unrecognized spatial and temporal variability. Thus, our results emphasize the need for
430 continuous, high-resolution observations of air-sea CO₂ fluxes, particularly in Arctic coastal

431 systems affected by stratification and meltwater input. These observations will be essential for
 432 refining flux parameterizations, reducing uncertainty in carbon budget estimates, and improving
 433 the representation of Arctic shelf systems in global carbon models.

434
 435 **Table 1.** CO₂ fluxes calculated based on pCO₂ measured at the different depth. The fluxes are
 436 calculated using the bulk model of Ho et al., 2006 and Nightingale et al. (2000). We have used
 437 locally measured wind speeds for the calculations to match flux measurements captured by eddy
 438 covariance.

Date	Depth (m)	Temperature (°C)	Salinity (psu)	pCO ₂ (µatm)	Wind Speed (m s ⁻¹)	Ho (2006)	Nightingale (2000)
						Flux (mmol CO ₂ m ⁻² day ⁻¹)	Flux (mmol CO ₂ m ⁻² day ⁻¹)
16-Jul	0.0	3.0 [†]	23	252 [‡]	6.8	-14.88	-13.69
16-Jul	0.1	3.0	23	244	6.8	-15.78	-14.52
16-Jul	1.0	1.8	26	240	6.8	-16.12	-14.83
16-Jul	2.0	1.1	28	241	6.8	-15.93	-14.66
16-Jul	4.0	0.3	29	275	6.8	-12.19	-11.21
18-Jul	0.0	6.0 [†]	7	262 [‡]	3.3	-3.45	-3.38
18-Jul	0.1	4.3	7	244	3.3	-3.98	-3.90
18-Jul	1.0	3.2	14	233	3.3	-4.20	-4.11
18-Jul	2.0	2.3	21	278	3.3	-2.86	-2.79
18-Jul	4.0	0.6	29	295	3.3	-2.34	-2.29
28-Jul	0.0	10.0 [†]	15	415 [‡]	2.5	0.53	0.54
28-Jul	0.1	10.0	15	405	2.5	0.38	0.38
28-Jul	1.0	7.0	21	365	2.5	-0.22	-0.23
28-Jul	2.0	5.0	27	282	2.5	-1.43	-1.45
28-Jul	4.0	2.0	30	290	2.5	-1.32	-1.34
31-Jul	0.0	12.0 [†]	15	401 [‡]	2.0	0.20	0.21
31-Jul	0.1	10.0	15	343	2.0	-0.36	-0.38
31-Jul	1.0	8.0	21	338	2.0	-0.40	-0.42
31-Jul	2.0	5.0	27	282	2.0	-0.92	-0.97
31-Jul	4.0	2.0	30	294	2.0	-0.81	-0.85

440

441 † Denotes skin temperatures derived from heat fluxes. ‡ Denotes pCO₂ values estimated from
442 measurements at 1 m depth and adjusted to derived skin temperatures.

443
444

445 **5 Conclusions**

446

447 During the summer thaw, carbon chemistry and pCO₂ dynamics in Arctic coastal surface waters
448 are significantly altered by the combined effects of snow and sea ice melt, terrestrial runoff, and
449 biological activity. These influences lead to substantial variability in surface temperature, pH,
450 dissolved inorganic carbon (DIC), and total alkalinity (TA), ultimately disrupting carbonate
451 system equilibrium in the upper water column. As a result, estimating air-sea CO₂ fluxes using
452 traditional bulk models becomes highly uncertain during this period.

453

454 The sea ice breakup period, typically lasting 2-4 weeks, represents a particularly dynamic and
455 complex phase in the annual cycle. Despite its brevity, this phase may have a disproportionate
456 influence on total summer CO₂ uptake, given that open-water conditions in high Arctic fjords are
457 limited to only 80-120 days per year (Sejr et al., 2011).

458

459 Air-sea gas exchange rates depend not only on the pCO₂ gradient between the atmosphere and
460 surface water, but also on rapid, nonlinear changes in surface water chemistry driven by the
461 composition and volume of meltwater and runoff. Accurate flux estimation will therefore require
462 knowledge of the depth at which surface water pCO₂ becomes vertically homogeneous,
463 combined with gas exchange parameterizations tailored to highly stratified and ice-affected
464 conditions. Profiling pCO₂ in the upper water column is therefore essential to identify this depth
465 and to constrain surface flux estimates reliably.

466

467 Several eddy covariance studies in other arctic environments report variable uptake and efflux of
468 CO₂ during the sea ice breakup period (e.g. Butterworth et al., 2025). Building on these findings,
469 our data provides the first step in understanding potential drivers behind this variability. Though,
470 proper quantification of the mechanisms driving nonlinear pCO₂ profiles and the resulting
471 uncertainty of flux estimates will require observations spanning the air-sea boundary. The
472 current lack of these datasets underscores the need for studies that integrate continuous, direct
473 CO₂ flux measurements with detailed observations of surface water carbonate chemistry,
474 atmospheric forcing, skin temperature, and turbulence at the air-ice-water interface.

475

476 Such integrated measurements are critical to improving our understanding of the drivers and net
477 effect of sea ice melt-driven changes on CO₂ fluxes in Arctic coastal systems. Ultimately, this
478 knowledge is essential to accurately quantify the seasonal and regional uptake of atmospheric
479 CO₂ in the rapidly changing Arctic.

480

481

482 **Acknowledgments**

483 This study is a contribution to the GreenFeedback project (Greenhouse gas fluxes and earth
484 system feedbacks, Grant agreement: 101056921), funded by the European Union under the
485 Horizon Europe program, who also supported L.L.S and H.C.H's involvement. H.C.H. was
486 additionally funded by the AUFF (Aarhus Universitets Forskningsfond, project no. AUFF-F-
487 2021-7-7) as part of his PhD. S.R. was funded by Aage V Jensens Fonde (grant no. AVJF21-
488 3012) and the Danish National Research Foundation (grant no. DNRF 185). MKS was funded by
489 the POMP project (Horizon Europe grant: 101136875) and the Connecting the Dots project
490 (Villum Foundation grant: 50110) D.H.S received financial support from the Greenland Climate
491 Research Centre (GCRC), Greenland Institute of Natural Resources. The study also received
492 financial support from The Danish Ministry of Climate, Energy and Utilities, Programme for
493 Arctic Climate, (project: Drivhusgas-observationer i Arktis (ObsArktis), 2017). Furthermore we
494 received support from The Arctic Research Centre, Aarhus University and Greenland Institute of
495 Natural Science. The authors especially wish to thank Egon Randa Frandsen, who assisted with
496 the logistics and the additional measurements in Young Sound. Additionally, the authors would
497 like to recognize the students in the EnCHil Nordic master program, who participated in taking
498 the Tasiilaq measurements. This work is a contribution to the Arctic Science Partnership (ASP)
499 and the MarinBasis component of the Greenland Ecosystem Monitoring Program.

500

501 **Author Contribution**

502 Conceptualization: LLS. Formal analysis, writing – original draft preparation: HCH. Funding
503 acquisition: LLS, SR, MKS, TP. Investigation: DS, BJ, KL, TP, MKS, JS, SR, LLS. Writing –
504 review and editing: DS, TP, MKS, SR, LLS. All the authors have read and agreed to the
505 published version of the paper.

506

507 **Data Availability Statement**

508 Vertical profiles from both Greenlandic fjords can be found in the Zenodo data repository:
509 <https://doi.org/10.5281/zenodo.17471918>

510

511 **Competing interests**

512 The authors declare no competing interests.

513

514

515 **References**

516

517 Ahmed, M. M. M., Else, B. G. T., Capelle, D., Miller, L. A., and Papakyriakou, T.: Underestimation of surface *p*
518 CO₂ and air-sea CO₂ fluxes due to freshwater stratification in an Arctic shelf sea, Hudson Bay, *Elementa: Science*
519 *of the Anthropocene*, 8, 084, <https://doi.org/10.1525/elementa.084>, 2020.

520 Arrigo, K. R. and van Dijken, G. L.: Continued increases in Arctic Ocean primary production, *Progress in*
521 *Oceanography*, 136, 60–70, <https://doi.org/10.1016/j.pocean.2015.05.002>, 2015.

- 522 Bates, N. R. and Mathis, J. T.: The Arctic Ocean marine carbon cycle: evaluation of air-sea CO₂ exchanges, ocean
523 acidification impacts and potential feedbacks, *Biogeosciences*, 6, 2433–2459, 2009.
- 524 Burgers, T. M., Miller, L. A., Thomas, H., Else, B. G. T., Gosselin, M., and Papakyriakou, T.: Surface Water CO₂
525 Variations and Sea-Air CO₂ Fluxes During Summer in the Eastern Canadian Arctic, *J. Geophys. Res. Oceans*, 122,
526 9663–9678, <https://doi.org/10.1002/2017jc013250>, 2017.
- 527 Butterworth, B. J., Else, B. G. T., Brown, K. A., Mundy, C. J., Williams, W. J., Rotermund, L. M., and de Boer, G.:
528 Annual carbon dioxide flux over seasonal sea ice in the Canadian Arctic, *EGU sphere*, 1–30,
529 <https://doi.org/10.5194/egusphere-2025-1802>, 2025.
- 530 de Caritat, P., Hall, G., Gislason, S., Belsey, W., Braun, M., Goloubeva, N. I., Olsen, H. K., Scheie, J. O., and Vaive,
531 J. E.: Chemical composition of arctic snow: concentration levels and regional distribution of major elements,
532 *Science of The Total Environment*, 336, 183–199, <https://doi.org/10.1016/j.scitotenv.2004.05.031>, 2005.
- 533 Dai, M., Su, J., Zhao, Y., Hofmann, E. E., Cao, Z., Cai, W.-J., Gan, J., Lacroix, F., Laruelle, G. G., Meng, F.,
534 Müller, J. D., Regnier, P. A. G., Wang, G., and Wang, Z.: Carbon Fluxes in the Coastal Ocean: Synthesis, Boundary
535 Processes, and Future Trends, *Annu. Rev. Earth Planet. Sci.*, 50, 593–626, <https://doi.org/10.1146/annurev-earth-032320-090746>, 2022.
- 537 Dong, Y., Yang, M., Bakker, D. C. E., Liss, P. S., Kitidis, V., Brown, I., Chierici, M., Fransson, A., and Bell, T. G.:
538 Near-Surface Stratification Due to Ice Melt Biases Arctic Air-Sea CO₂ Flux Estimates, *Geophysical Research*
539 *Letters*, 48, <https://doi.org/10.1029/2021GL095266>, 2021.
- 540 Garbe, C. S., Rutgersson, A., Boutin, J., de Leeuw, G., Delille, B., Fairall, C. W., Gruber, N., Hare, J., Ho, D. T.,
541 Johnson, M. T., Nightingale, P. D., Pettersson, H., Piskozub, J., Sahlée, E., Tsai, W., Ward, B., Woolf, D. K., and
542 Zappa, C. J.: Transfer Across the Air-Sea Interface, in: *Ocean-Atmosphere Interactions of Gases and Particles*,
543 edited by: Liss, P. S. and Johnson, M. T., Springer, Berlin, Heidelberg, 55–112, https://doi.org/10.1007/978-3-642-25643-1_2, 2014.
- 545 Gattuso, J.-P., Epitalon, J.-M., Lavigne, H., Orr, J., Gentili, B., Hagens, M., Hofmann, A., Mueller, J.-D., Proye, A.,
546 Rae, J., and Soetaert, K.: *seacarb: Seawater Carbonate Chemistry*, 2024.
- 547 Geilfus, N.-X., Carnat, G., Papakyriakou, T., Tison, J.-L., Else, B., Thomas, H., Shadwick, E., and Delille, B.:
548 Dynamics of pCO₂ and related air-ice CO₂ fluxes in the Arctic coastal zone (Amundsen Gulf, Beaufort Sea), *J.*
549 *Geophys. Res.*, 117, n/a-n/a, <https://doi.org/10.1029/2011JC007118>, 2012.
- 550 Geilfus, N.-X., Galley, R. J., Crabeck, O., Papakyriakou, T., Landy, J., Tison, J.-L., and Rysgaard, S.: Inorganic
551 carbon dynamics of melt-pond-covered first-year sea ice in the Canadian Arctic, *Biogeosciences*, 12, 2047–2061,
552 <https://doi.org/10.5194/bg-12-2047-2015>, 2015.
- 553 Granskog, M. A., Kuzyk, Z. Z. A., Azetsu-Scott, K., and Macdonald, R. W.: Distributions of runoff, sea-ice melt
554 and brine using $\delta^{18}\text{O}$ and salinity data — A new view on freshwater cycling in Hudson Bay, *Journal of Marine*
555 *Systems*, 88, 362–374, <https://doi.org/10.1016/j.jmarsys.2011.03.011>, 2011.
- 556 Hansen, J. W., Thamdrup, B., and Jørgensen, B. B.: Anoxic incubation of sediment in gas-tight plastic bags: a
557 method for biogeochemical process studies, *Marine Ecology Progress Series*, 208, 273–282, 2000.
- 558 Haraldsson, C., Anderson, L. G., Hassellöv, M., Hulth, S., and Olsson, K.: Rapid, high-precision potentiometric
559 titration of alkalinity in ocean and sediment pore waters, *Deep Sea Research Part I: Oceanographic Research Papers*,
560 44, 2031–2044, [https://doi.org/10.1016/S0967-0637\(97\)00088-5](https://doi.org/10.1016/S0967-0637(97)00088-5), 1997.
- 561 Henson, H. C., Holding, J. M., Meire, L., Rysgaard, S., Stedmon, C. A., Stuart-Lee, A., Bendtsen, J., and Sejr, M.:
562 Coastal freshening drives acidification state in Greenland fjords, *Science of The Total Environment*, 855, 158962,
563 <https://doi.org/10.1016/j.scitotenv.2022.158962>, 2023.

- 564 Henson, H. C., Sejr, M., Meire, L., Sørensen, L. L., Winding, M. H. S., and Holding, J. M.: Resolving Heterogeneity
565 in CO₂ Uptake Potential in the Greenland Coastal Ocean, *Journal of Geophysical Research: Biogeosciences*, 129,
566 e2024JG008246, <https://doi.org/10.1029/2024JG008246>, 2024.
- 567 Henson, H. C., Puts, I. C., Sejr, M. K., Sørensen, L. L., and Holding, J. M.: Glacial meltwater increases coastal
568 carbon dioxide uptake and sensitivity to biogeochemical change, *Commun Earth Environ*, 6, 687,
569 <https://doi.org/10.1038/s43247-025-02685-4>, 2025.
- 570 Jørgensen, H. E., Sørensen, L. L., and Larsen, S. E.: A Simple Model of Chemistry Effects on the Air-Sea CO₂
571 Exchange Coefficient, *Journal of Geophysical Research: Oceans*, 125, e2018JC014808,
572 <https://doi.org/10.1029/2018JC014808>, 2020.
- 573 Laruelle, G. G., Lauerwald, R., Pfeil, B., and Regnier, P.: Regionalized global budget of the CO₂ exchange at the
574 air-water interface in continental shelf seas, *Global Biogeochemical Cycles*, 28, 1199–1214,
575 <https://doi.org/10.1002/2014GB004832>, 2014.
- 576 Liss, P. S. and Slater, P. G.: Flux of Gases across the Air-Sea Interface, *Nature*, 247, 181–184,
577 <https://doi.org/10.1038/247181a0>, 1974.
- 578 Lueker, T. J., Dickson, A. G., and Keeling, C. D.: Ocean pCO₂ calculated from dissolved inorganic carbon,
579 alkalinity, and equations for K₁ and K₂: validation based on laboratory measurements of CO₂ in gas and seawater at
580 equilibrium, *Marine Chemistry*, 70, 105–119, [https://doi.org/10.1016/s0304-4203\(00\)00022-0](https://doi.org/10.1016/s0304-4203(00)00022-0), 2000.
- 581 Meire, L., Søgaard, D. H., Mortensen, J., Meysman, F. J. R., Soetaert, K., Arendt, K. E., Juul-Pedersen, T., Blicher,
582 M. E., and Rysgaard, S.: Glacial meltwater and primary production are drivers of strong
583 CO₂ uptake in fjord and coastal waters adjacent to the Greenland Ice Sheet,
584 *Biogeosciences*, 12, 2347–2363, <https://doi.org/10.5194/bg-12-2347-2015>, 2015.
- 585 Meire, L., Mortensen, J., Meire, P., Juul-Pedersen, T., Sejr, M. K., Rysgaard, S., Nygaard, R., Huybrechts, P., and
586 Meysman, F. J. R.: Marine-terminating glaciers sustain high productivity in Greenland fjords, *Glob Change Biol*, 23,
587 5344–5357, <https://doi.org/10.1111/gcb.13801>, 2017.
- 588 Miller, L. A., Papakyriakou, T. N., Collins, R. E., Deming, J. W., Ehn, J. K., Macdonald, R. W., Mucci, A., Owens,
589 O., Raudsepp, M., and Sutherland, N.: Carbon dynamics in sea ice: A winter flux time series, *J. Geophys. Res.*, 116,
590 C02028, <https://doi.org/10.1029/2009JC006058>, 2011.
- 591 Miller, L. A., Burgers, T. M., Burt, W. J., Granskog, M. A., and Papakyriakou, T. N.: Air-Sea CO₂ Flux Estimates
592 in Stratified Arctic Coastal Waters: How Wrong Can We Be?, *Geophys. Res. Lett.*, 46, 235–243,
593 <https://doi.org/10.1029/2018gl080099>, 2019.
- 594 Nomura, D., Yoshikawa-Inoue, H., Toyota, T., and Shirasawa, K.: Effects of snow, snowmelting and refreezing
595 processes on air–sea-ice CO₂ flux, *Journal of Glaciology*, 56, 262–270,
596 <https://doi.org/10.3189/002214310791968548>, 2010.
- 597 Perovich, D., Meier, W., Tschudi, M., Hendricks, S., Petty, A. A., Divine, D., Farrell, S., Gerland, S., Haas, C.,
598 Kaleschke, L., Pavlova, O., Ricker, R., Tian-Kunze, X., Webster, M., and Wood, K.: Arctic Report Card 2020: Sea
599 Ice, 2020.
- 600 Raimondi, L., Matthews, J. B. R., Atamanchuk, D., Azetsu-Scott, K., and Wallace, D. W. R.: The internal
601 consistency of the marine carbon dioxide system for high latitude shipboard and *in situ* monitoring, *Marine*
602 *Chemistry*, 213, 49–70, <https://doi.org/10.1016/j.marchem.2019.03.001>, 2019.
- 603 Roobaert, A., Laruelle, G. G., Landschützer, P., Gruber, N., Chou, L., and Regnier, P.: The Spatiotemporal
604 Dynamics of the Sources and Sinks of CO₂ in the Global Coastal Ocean, *Global Biogeochemical Cycles*, 33, 1693–
605 1714, <https://doi.org/10.1029/2019GB006239>, 2019.

- 606 Rysgaard, S., Vang, T., Stjernholm, M., Rasmussen, B., Windelin, A., and Kiilsholm, S.: Physical Conditions,
607 Carbon Transport, and Climate Change Impacts in a Northeast Greenland Fjord, Arctic, Antarctic, and Alpine
608 Research, 35, 301–312, [https://doi.org/10.1657/1523-0430\(2003\)035%255B0301:PCCTAC%255D2.0.CO;2](https://doi.org/10.1657/1523-0430(2003)035%255B0301:PCCTAC%255D2.0.CO;2), 2003.
- 609 Rysgaard, S., Søgaard, D. H., Cooper, M., Pu´co, M., Lennert, K., Papakyriakou, T. N., Wang, F.,
610 Geilfus, N. X., Glud, R. N., Ehn, J., McGinnis, D. F., Attard, K., Sievers, J., Deming, J. W., and Barber, D.: Ikaite
611 crystal distribution in winter sea ice and implications for CO₂ system dynamics, *The Cryosphere*, 7, 707–718,
612 <https://doi.org/10.5194/tc-7-707-2013>, 2013.
- 613 Sejr, Krause-Jensen, D., Rysgaard, S., Sørensen, L. L., Christensen, P. B., and Glud, R. N.: Air—sea flux of CO₂ in
614 arctic coastal waters influenced by glacial melt water and sea ice, *Tellus B: Chemical and Physical Meteorology*, 63,
615 815–822, <https://doi.org/10.1111/j.1600-0889.2011.00540.x>, 2011.
- 616 Sejr, M. K., Stedmon, C. A., Bendtsen, J., Abermann, J., Juul-Pedersen, T., Mortensen, J., and Rysgaard, S.:
617 Evidence of local and regional freshening of Northeast Greenland coastal waters, *Sci Rep*, 7, 13183,
618 <https://doi.org/10.1038/s41598-017-10610-9>, 2017.
- 619 Semiletov, I., Makshtas, A., Akasofu, S., and L Andreas, E.: Atmospheric CO₂ balance: The role of Arctic sea ice,
620 *Geophysical Research Letters*, 31, 2003GL017996, <https://doi.org/10.1029/2003GL017996>, 2004.
- 621 Sievers, Papakyriakou, T., Larsen, S. E., Jammet, M. M., Rysgaard, S., Sejr, M., and Sørensen, L. L.: Estimating
622 surface fluxes using eddy covariance and numerical ogive optimization, *Atmospheric Chemistry and Physics*, 15,
623 2081–2103, <https://doi.org/10.5194/acp-15-2081-2015>, 2015a.
- 624 Sievers, J., Papakyriakou, T., Larsen, S. E., Jammet, M. M., Rysgaard, S., Sejr, M. K., and Sørensen, L. L.:
625 Estimating surface fluxes using eddy covariance and numerical ogive optimization, *Atmospheric Chemistry and*
626 *Physics*, 15, 2081–2103, <https://doi.org/10.5194/acp-15-2081-2015>, 2015b.
- 627 Smedman, A., Högström, U., Sahlée, E., and Cecilia, J.: Critical re-evaluation of the bulk transfer coefficient for
628 sensible heat over the ocean during unstable and neutral conditions, *Quart J Royal Meteorol Soc*, 133, 227–250,
629 <https://doi.org/10.1002/qj.6>, 2007.
- 630 Søgaard, D. H., Thomas, D. N., Rysgaard, S., Glud, R. N., Norman, L., Kaartokallio, H., Juul-Pedersen, T., and
631 Geilfus, N.-X.: The relative contributions of biological and abiotic processes to carbon dynamics in subarctic sea
632 ice, *Polar Biol*, 36, 1761–1777, <https://doi.org/10.1007/s00300-013-1396-3>, 2013.
- 633 Søgaard, D. H., Sorrell, B. K., Sejr, M. K., Andersen, P., Rysgaard, S., Hansen, P. J., Skyttä, A., Lemcke, S., and
634 Lund-Hansen, L. C.: An under-ice bloom of mixotrophic haptophytes in low nutrient and freshwater-influenced
635 Arctic waters, *Sci Rep*, 11, 2915, <https://doi.org/10.1038/s41598-021-82413-y>, 2021.
- 636 Sulpis, O., Lauvset, S. K., and Hagens, M.: Current estimates of K₁* and K₂* appear inconsistent with measured
637 CO₂ system parameters in cold oceanic regions, *Ocean Science*, 16, 847–862, [https://doi.org/10.5194/os-16-847-](https://doi.org/10.5194/os-16-847-2020)
638 2020, 2020.
- 639 Wanninkhof, R., Asher, W., Ho, D., Sweeney, C., and McGillis, W.: Advances in Quantifying Air-Sea Gas
640 Exchange and Environmental Forcing*, *Annual review of marine science*, 1, 213–44,
641 <https://doi.org/10.1146/annurev.marine.010908.163742>, 2009.
- 642 Watts, J., Bell, T. G., Anderson, K., Butterworth, B. J., Miller, S., Else, B., and Shutler, J.: Impact of sea ice on air-
643 sea CO₂ exchange – A critical review of polar eddy covariance studies, *Progress in Oceanography*, 201, 102741,
644 <https://doi.org/10.1016/j.pocean.2022.102741>, 2022.
- 645 Woolf, D. K., Land, P. E., Shutler, J. D., Goddijn-Murphy, L. M., and Donlon, C. J.: On the calculation of air-sea
646 fluxes of CO₂ in the presence of temperature and salinity gradients, *Journal of Geophysical Research: Oceans*, 121,
647 1229–1248, <https://doi.org/10.1002/2015JC011427>, 2016.

